Thin-Walled Structures 94 (2015) 67–78

Contents lists available at ScienceDirect

Thin-Walled Structures

journal homepage: www.elsevier.com/locate/tws

Predictive models of the flexural overstrength factor for steel thin-walled circular hollow section beams

Mario D'Aniello [a], Esra Mete Güneyisi [b,*], Raffaele Landolfo [a], Kasım Mermerdaş [c]

[a] Department of Structures for Engineering and Architecture, University of Naples "Federico II", Naples, Italy
[b] Department of Civil Engineering, Gaziantep University, Gaziantep, Turkey
[c] Department of Civil Engineering, Hasan Kalyoncu University, Gaziantep, Turkey

ARTICLE INFO

Article history:
Received 24 February 2015
Accepted 20 March 2015
Available online 22 April 2015

Keywords:
Circular hollow section
Experimental database
Modelling
Overstrength factor
Steel beam
Genetic algorithm

ABSTRACT

Circular hollow section (CHS) steel beams are widely used in both mechanical and civil applications. CHS members are mainly subjected to bending. The flexural overstrength factor (namely the ratio between the ultimate bending strength over the plastic bending moment) characterizes the flexural behaviour of steel CHS beams. This paper describes an analytical study aiming to develop a new explicit formulation for predicting the flexural overstrength factor of steel CHS beams. The proposed models were derived from soft-computing techniques based on both neural networks (NNs) and gene expression programming (GEP), respectively. To this aim, experimental data available from scientific literature were analysed and collected to form a comprehensive dataset for developing the prediction models. A total number of 128 samples was considered in order to cover different geometric and mechanical properties. The input variables accounted for the modelling were the external diameter (D), wall thickness (t), shear length (L_v), and steel yield strength (f_y). The database was arbitrarily divided into two subsets to obtain both training and testing databases for the generation of the models. The prediction capability of the proposed formulations was assessed with respect to the experimental data and the levels of accuracy and performance were also compared with an existing analytical formulation available previously developed for cold-formed sections. The results showed that the novel proposed models derived from NN and GEP methods provide better prediction performances than those obtained by the existing analytical model.

1. Introduction

Steel circular hollow sections (CHS) are widely used in civil structures (e.g. buildings, bridges, wind towers, off-shore structures, land-based pipelines, etc.) thanks to their efficient geometry and aesthetically pleasing over open cross section shapes. Moreover, CHS members are also extensively adopted in mechanical applications (e.g. piping, vehicle trailers, fences and handrails, etc.) because of their higher strength-to-weight ratio than conventional sections, which enhances efficiency and reduces costs.

The wide range of applications for CHS members implies that these types of members should be design to resist various loading conditions and combinations such as axial forces, bending moments, and torsion [1]. However, CHS are generally prone to the ovalization of cross-section (which can be defined as the ratio of change of the outside diameter to original outside diameter) due to bending actions, which is anticipated by local buckling and characterized by significant alterations of cross section profile along the tube length, thus impairing both the flexural stiffness and the ultimate capacity. Therefore, the prediction of ultimate flexural performance of circular steel tubes has a key role in many structural applications [2–4].

The main response parameters governing the bending behaviour of steel beams are the rotation capacity (r) and flexural overstrength (s) [5–7], which are defined in Fig. 1. Especially for the earthquake-resistant design, such parameters are crucial to assure both the adequate energy dissipation capacity and the effectiveness of hierarchy criteria. In particular, r is the source of the beam ductility, which needs to achieve a global dissipative structural behaviour, while s governs the flexural overstrength, which must be accurately known to apply capacity design principles, as currently recommended by modern seismic codes.

At the Authors' knowledge, the analytical estimation of the rotation capacity and flexural overstrength factor of the CHS steel beams has not been studied comprehensively in the literature even though numerous studies have been carried out to obtain analytical formulations for predicting such response parameters of steel members with other cross section geometries (i.e., I–H section and rectangular and square hollow sections (RHS–SHS)).

* Corresponding author. Tel.: +90 342 3172423; fax: +90 342 3601107.
E-mail address: eguneyisi@gantep.edu.tr (E.M. Güneyisi).

http://dx.doi.org/10.1016/j.tws.2015.03.020
0263-8231/

List of symbols

a	normalization coefficient for outputs
b	normalization coefficient for outputs
f_{LB}	stress corresponding to the complete development of local buckling
f_y	yielding stress
m_i	measured values
m'	mean values of measured values
p_i	predicted values
p'	mean values of predicted values
r	rotation capacity
s	flexural overstrength
t	thickness of the tube
w_i	weight
D	diameter of the tube
E	modulus of elasticity
I_i	inputs
L	beam length
L_v	shear length of the beam
M_{max}	maximum moment that can be developed by the beam
M_p	full plastic moment
R	correlation coefficient
α	slenderness parameter
β	actual input parameter or output values
$\beta_{normalized}$	normalized value of input parameters or outputs
β_{max}	maximum actual values of either inputs or outputs
β_{min}	minimum actual values of either inputs or outputs

List of acronyms

CBT	cantilever bending test
CHS	circular hollow sections
ET	expression tree
GA	genetic algorithm
GEP	gene expression programming
GP	genetic programming
MAPE	mean absolute percent error
MSE	mean square error
NN	neural network
PBT	point bending test
RHS	rectangular hollow section
RMSE	root mean square error
SHS	square hollow section

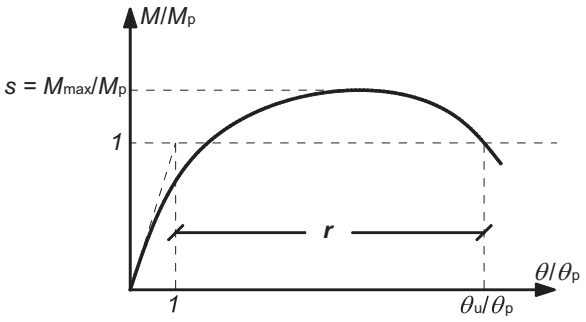

Fig. 1. Generalized moment–rotation curve for a steel beam [5].

For example, in the study of Wilkinson and Hancock [8], a finite element analysis was used to predict the rotation capacity of cold-formed RHS beams. Gioncu et al. [9] and Anastasiadis et al. [10] developed a computer programme (DUCTROT-M) to compute both the flexural strength and available rotation capacity of I beams. Recently, soft-computing based methods has also been applied on the field of steel beams by D'Aniello et al. [11] to estimate the available rotation capacity of cold-formed RHS–SHS steel beams. In another study, the Authors [12,13] proposed analytical formulation of the flexural overstrength of the steel beams fabricated with I–H section and RHS–SHS using soft computing techniques.

For what concerns the bending behaviour of the steel CHS beams, various types of manufactured tubes (e.g. hot-formed, cold-formed, and welded fabricated tubes) have been experimentally investigated considering different types of loading conditions and boundary conditions (i.e., simply-supported, cantilever, and pure bending beam tests) [14–22]. The review of these studies reveals that different geometrical and mechanical properties were experimentally evaluated. However, poor attention was addressed on the mathematical modelling of the CHS beams. Due to the high non-linearity and complexity of the ultimate response of circular tubes under pure bending, the accurate prediction of the ultimate bending strength of steel CHS beams using conventional analytical solutions requires rigorous mathematical procedures [4] incorporating simplified assumptions which affect the accuracy of the predicted performance.

An alternative approach that allows overcoming the limits of analytical solutions is the implementation of numerical finite element analyses. With this regard, numerical studies based on three-dimensional nonlinear finite-element models have been carried out to estimate the load-deformation response and ultimate strength of seam-welded structural stainless steel CHS beams subjected to bending [23].

Recently, two studies conducted by Shahin and Elchalakani [24,25] showed the feasibility of using both polynomial regression and neural network for modelling the ultimate pure bending of steel circular tubes. They demonstrated that these mathematical techniques are very efficient and are not affected by any assumptions or simplifications, enabling the limitations of most existing modelling techniques to be overcome since these techniques do not need predefined mathematical equations of the relationship between the model inputs and corresponding outputs.

The above consideration motivated the Authors to propose novel mathematical models based on soft computing techniques for the flexural overstrength factor of steel CHS beams. In order to achieve this purpose, two soft-computing methods were implemented, namely (i) neural network and (ii) gene expression programming approaches. The mathematical models were developed using a wide experimental database (covering 128 test results) that was collected from the review of the existing literature. The accuracy of the proposed models was also verified against the experimental data and the rates of efficiency were compared with the linear regression-based model developed by Kato [26,27].

2. Flexural overstrength factor

The flexural overstrength factor "s" is a non-dimensional parameter representing the ratio between the critical stress that brings to the local instability and the yielding stress. It is generally intended to be utilized for measuring the ultimate bending

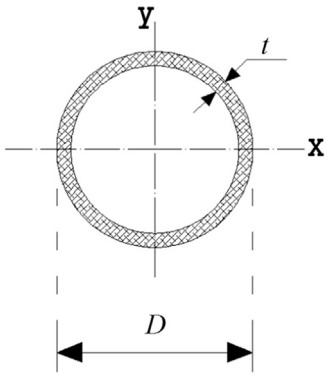

Fig. 2. Geometry of circular hollow section.

capacity of steel beams. This factor can be calculated by the following relation:

$$s=\frac{f_{LB}}{f_y} \tag{1}$$

where f_{LB} is the stress corresponding to the complete development of local buckling and f_y is the yielding stress. However, this parameter can also be calculated using the following more practical expression:

$$s=\frac{M_{\max}}{M_p} \tag{2}$$

where $M_{\max}$ represents the maximum moment that can be reached by the structure while M_p is the theoretical full plastic moment. The description is also given in the generalized moment −rotation curve of a member able to withstand plastic deformation shown in Fig. 1. It is important to note that the ultimate capacity of steel beams can be significantly larger than the plastic bending strength because of the strain hardening that can be developed just before the complete local buckling or fractures [5].

As previously mentioned, there have been several studies focusing on the analytical formulation of the flexural overstrength of the I–H section and RHS–SHS steel beams in the literature [5,6,12,26,27]. However, the studies on the flexural overstrength factor of CHS beams are very limited. In the literature, based on the experimental test results conducted on cold-formed CHS members, Kato [26,27] proposed the following empirical relation to determine the flexural overstrength of the CHS:

$$\frac{1}{s}=0.777+\frac{1.18}{\alpha} \tag{3}$$

$$\alpha=\frac{E}{f_y}\left(\frac{t}{D}\right)^2 \tag{4}$$

where s is the overstrength factor, α is the slenderness parameter, E is the modulus of elasticity, f_y is the yield strength, while D and t are the diameter and the thickness of the CHS, respectively, (see Fig. 2).

3. Experimental database used for derivation of the models

The proposed formulations of s for circular hollow section steel beams were derived using a set of 128 experimental data available in the technical literature [14–22]. The data sources and the brief information regarding the test configurations are given in Table 1. Moreover, Fig. 3 shows the bending test configurations used in the reference works reported in Table 1. The details of critical predictive parameters, namely, diameter of the section (D), thickness (t), shear length of the beam (L_v) (being equal to $L/2$ for 3PBT, $(L_1-L_2)/2$ for 4PBT and PBT, and L for CBT where L, L_1, L_2 are described in Fig. 3), and yield strength of the steel (f_y) are given in Table 2 for each data sample as well as the corresponding flexural overstrength factor (s).

Table 1
Available experimental data on bending test of CHS steel beams.

No.	Reference	Test no.	Fabrication type	Loading type	Loading history
1	Sedlacek et al. [14]	32	Hot-formed	3PBT[a]/ 4PBT[b]	Monotonic
2	Elchalakani et al. [15]	12	Cold-formed	PBT[c]	Monotonic
3	Elchalakani et al. [16]	9	Cold-formed	PBT	Monotonic
4	Jiao and Zhao [17]	12	Cold-formed	4PBT/PBT	Monotonic
5	Elchalakani et al. [18]	25	Cold-formed	PBT	Cycling
6	Kıymaz [19]	8	Fabricated	4PBT	Monotonic
7	Elchalakani et al. [20]	9	Cold-formed	PBT	Cycling
8	Haedir et al. [21]	5	Cold-formed	PBT	Monotonic
9	Guo et al. [22]	16	Fabricated	4PBT/CBT[d]	Monotonic

[a] 3PBT=3-point bending test.
[b] 4PBT=4-point bending test.
[c] PBT=Pure bending test.
[d] CBT=cantilever bending test.

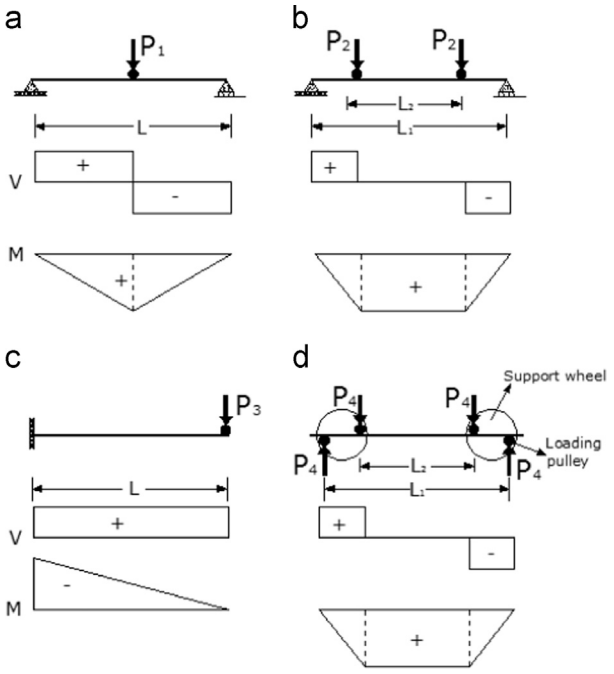

Fig. 3. Bending test configurations and corresponding shear/moment diagrams for (a) 3-point bending test (3PBT), (b) 4-point bending test (4PBT), (c) cantilever bending test (CBT), and (d) pure bending test (PBT).

The statistical analysis of the input and output data given in Table 2 is presented in Table 3, indicating that the data samples were selected in an order to establish a consistent sequence of the inputs to be used for derivation of the models. The input nodes cover the wide range and statistical variation for the geometric properties of the section, mechanical properties of the material, as well as the shear length of the steel beams.

The data set was randomly divided into two parts to obtain training and testing databases in the modelling. Hence, about one fourth of the total data samples (i.e. 32) were considered to be the test database, while the rest was used as training database (i.e. 96).

Table 2
The experimental database used for the model development.

Ref no.	Data no.	D (mm)	t (mm)	L_v (mm)	f_y (MPa)	s_{exp}
[14]	1	219.01	4.51	850	290	1.02
	2	219.25	4.4	1350	290	0.97
	3	121.28	7.23	850	309	1.27
	4	121.4	7.19	1350	309	1.20
	5	220.13	6.01	850	309	1.04
	6	220.03	5.89	1350	309	0.95
	7	193.72	12.53	850	560	1.44
	8	193.7	12.28	1350	560	1.40
	9	121.33	7.41	850	402	1.25
	10	121.16	7.2	1350	402	1.38
	11	246.2	6.99	850	412	1.10
	12	246.18	7.28	1350	412	1.08
	13	246.28	8.34	850	373	1.21
	14	246.38	8.21	1350	373	1.23
	15	133.59	3.76	1000	304	1.11
	16	133.44	3.77	1000	304	0.94
	17	177.99	4.73	1000	341	1.16
	18	178.02	4.75	1000	341	1.00
	19	219.08	4.32	1000	290	1.10
	20	219.03	4.38	1000	290	0.97
	21	139.66	5.09	1000	495	1.22
	22	139.67	5.19	1000	495	1.00
	23	139.72	7.34	1000	478	1.27
	24	139.73	7.53	1000	478	1.03
	25	168.2	8.18	1000	488	1.25
	26	168.35	8.35	1000	488	1.01
	27	133.24	3.96	1000	440	1.13
	28	133.21	3.96	1000	440	0.97
	29	133.36	5.63	1000	373	1.30
	30	133.18	5.63	1000	373	1.15
	31	219.32	4.53	1000	471	1.06
	32	219.32	4.53	1000	471	1.00
[15]	33	110.1	1.1	300	408	0.73
	34	109.9	1	300	408	0.76
	35	109.7	0.9	300	408	0.79
	36	110.4	1.25	300	408	0.75
	37	98.6	1.7	300	410	0.99
	38	98.8	1.2	300	404	0.81
	39	99.2	1.4	300	404	1.01
	40	99.6	1.6	300	404	0.96
[15]	41	100	1.8	300	365	0.84
	42	99.8	2.3	300	410	1.11
	43	87.3	2.4	300	412	0.80
	44	100.6	2.1	300	404	0.90
[16]	45	101.6	2.6	300	365	0.96
	46	88.9	2.6	300	432	0.90
	47	76.1	2.3	300	415	0.91
	48	88.9	3.2	300	412	0.97
	49	60.3	2.3	300	433	0.86
	50	76.1	3.2	300	456	0.97
	51	60.3	2.9	300	408	1.02
	52	33.7	2.0	300	442	0.92
	53	33.7	2.6	300	460	0.96
[17]	54	31.86	1.56	400	1327	1.13
	55	31.86	1.76	400	1284	1.12
	56	31.93	1.96	400	1350	1.10
	57	38.04	1.58	400	1398	1.11
	58	38.16	1.78	400	1361	1.14
	59	38.06	1.98	400	1330	1.14
	60	57.15	1.58	400	1360	1.09
	61	75.95	1.59	400	1377	0.97
	62	31.76	1.97	300	1350	1.09
	63	38.1	1.97	300	1330	1.15
	64	57.08	1.56	300	1360	1.05
	65	75.98	1.59	300	1377	0.94
[18]	66	101.8	2.44	300	365	0.99
	67	89.3	2.52	300	378	0.89
	68	76.3	2.17	300	415	0.94
	69	89.3	3.10	300	412	0.99
	70	60.7	2.23	300	433	0.92
	71	76.2	3.07	300	456	1.03
	72	60.7	2.90	300	408	0.93
	73	33.8	2.40	300	460	1.04
	74	101.8	2.44	300	365	0.99

Table 2 (*continued*)

Ref no.	Data no.	D (mm)	t (mm)	L_v (mm)	f_y (MPa)	s_{exp}
	75	101.8	2.44	300	378	0.93
	76	89.3	2.52	300	415	0.94
	77	89.1	3.08	300	473	0.92
	78	60.2	2.29	300	407	1.05
	79	76.2	3.07	300	456	0.99
	80	60.37	2.95	300	413	0.99
	81	101.1	2.54	300	400	1.07
	82	89.3	2.52	300	378	1.00
	83	76.1	2.35	300	370	0.96
	84	89.1	3.08	300	473	0.98
	85	60.2	2.29	300	407	1.06
	86	75.9	3.13	300	402	1.01
	87	60.4	2.95	300	413	1.06
	88	89.3	2.52	300	378	1.01
	89	60.23	2.29	300	407	1.21
	90	60.4	2.95	300	413	1.14
[19]	91	103.3	1.4	750	469	1.06
	92	152.6	1.3	750	458	0.94
	93	202.9	1.4	750	375	0.90
	94	218.4	1.8	750	337	0.98
	95	114.7	2.7	750	643	1.02
	96	169	3.7	750	602	1.01
	97	219.5	3	750	598	0.75
	98	220.1	3.8	750	560	1.05
[20]	99	101.1	2.54	300	400	0.89
	100	89.3	2.52	300	378	0.90
	101	76.1	2.35	300	370	0.91
	102	89.1	3.08	300	473	0.91
	103	60.2	2.29	300	407	1.05
	104	75.9	3.13	300	402	0.88
	105	60.4	2.95	300	413	1.02
	106	89.3	2.52	300	378	0.86
	107	60.4	2.95	300	413	1.00
[21]	108	33.82	2.7	300	479	1.05
	109	86.46	1.97	300	455	0.87
	110	85.13	1.31	300	470	0.74
	111	84.73	1.11	300	457	0.74
	112	84.4	0.94	300	457	0.69
[22]	113	150	2	1000	190	1.05
	114	150	2	1000	190	1.03
	115	200	2	1000	190	1.00
	116	200	2	1000	190	1.02
	117	250	2	1200	190	1.01
	118	250	2	1200	190	1.01
	119	300	2	1200	190	0.95
	120	300	2	1200	190	0.94
	121	200	2	1500	190	1.02
	122	200	2	1500	190	1.03
	123	400	2	2000	190	0.86
	124	400	2	2000	190	0.77
	125	600	2	3000	190	0.85
	126	600	2	3000	190	0.68
	127	400	2	2000	190	1.09
	128	600	2	3000	190	1.00

In the next sections, the effectiveness of the correlation between the experimental and predicted flexural overstrength factor is evaluated by means of the correlation coefficient "R" (see Eq. (5)), which describes the fit of the models' output variable approximation curve to the actual test data output variable curve. Higher R coefficient indicates a model with better output approximation capability.

$$R = \frac{\sum (m_i - m')(p_i - p')}{\sqrt{\sum (m_i - m')^2 \sum (p_i - p')^2}} \tag{5}$$

where m' and p' are mean values of measured (m_i) and predicted (p_i) values, respectively.

4. Overview of soft-computing techniques

According to Zadeh [28], soft-computing is a collection of methodologies aiming to exploit the tolerance for imprecision and uncertainty to achieve tractability, robustness, and low solution cost. The model of reference for soft-computing is the human mind. Fuzzy logic, neuro-computing, and probabilistic reasoning are the main components of soft-computing. There are several fields of application for soft-computing techniques. Among the most popular methods, neural network (NN) and genetic programming (GP) were selected in this study and used to develop a mathematical model to estimate the flexural overstrength factor for circular hollow section (CHS) beams.

4.1. Fundamental aspects of genetic programming

Genetic programming (GP) is basically an application of genetic algorithms to computer programs and it can be considered as an extension of the genetic algorithm into the arena of computer programs [29]. GP is a domain-independent method that is inspired by biological evolution, which genetically breeds a population of computer programs to solve a problem performing a task defined by a user. Indeed, genetic programming iteratively transforms a population of computer programs into a new generation of programs by applying analogues of naturally occurring genetic operations. The genetic operations include crossover, mutation, reproduction, gene duplication, and gene deletion. Analogues of developmental processes that transform an embryo into a fully developed entity are also employed.

GP has been applied successfully to solve discrete, non-differentiable, combinatory, and general nonlinear engineering optimization problems [30].

Gene expression programming (GEP) was introduced by Ferreira [31] and it can be considered as a natural development of genetic algorithms and genetic programming. GEP evolves a computer program of different sizes and shapes encoded in linear chromosomes of fixed-length. The first step of a GEP algorithm is the random generation of the fixed-length chromosomes of each individual for the initial population. Then, the chromosomes are expressed and the fitness of each individual is evaluated based on the quality of the solution it represents. In this study, the GEP based mathematical model was derived using the GeneXpro-Tools.4.0 software.

Table 3
Descriptive statistics for the experimental data used in the model.

	D (mm)	t (mm)	L_v (mm)	f_y (MPa)	s_{exp}
Sample size	128	128	128	128	128
Mean	137.96	3.24	692.19	475.40	1.01
Standard error	9.30	0.19	49.16	26.36	0.01
Standard deviation	105.17	2.15	556.19	298.20	0.14
Variance	11,061.07	4.60	309,347.93	88,926.18	0.02
COV	0.76	0.66	0.80	0.63	0.14
Kurtosis	7.45	4.51	5.39	4.44	0.88
Skewness	2.39	2.00	2.03	2.30	0.35
Min. value	31.76	0.90	300.00	190.00	0.68
Max. value	600.00	12.53	3000.00	1398.00	1.44
Range	568.24	11.63	2700.00	1208.00	0.76
Midrange	315.88	6.72	1650.00	794.00	1.06
Sum	17,659.43	414.13	88,600.00	60,851.00	128.72

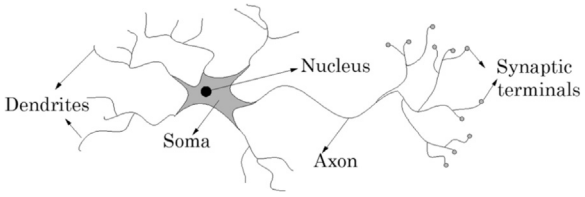

Fig. 4. Simplified model of a biological neuron [33].

4.2. Fundamental aspects of neural networks

An artificial neural network (NN) is a computational system that simulates the microstructure of a biological nervous system, such as the brain [32]. Therefore, the terminology used for NN is derived from the neuroscience. With this regard, Fig. 4 indicates the basic components of a natural neuron [33]. The perception process capacity of the brain depends on both the numbers of these basic components and the multiple connections among them. The key element of information processing paradigm is the novel structure of the information processing system. It is composed of a large number of highly interconnected processing elements (neurons) working in unison to solve specific problems. Consistently with biological neurons, NN uses artificial neurons to provide machine learning system. In particular, as for biological systems, the learning process involves adjustments to the synaptic connections between the neurons.

The artificial neuron is made of three main components, namely the weights, bias, and an activation function. Each neuron receives inputs $I_1, I_2,\ldots, I_n$ attached with a weight w_i which displays the connection strength for that input for each connection. Each input is then multiplied by the corresponding weight of the neuron connection. A bias can be defined as a type of connection weight with a constant nonzero value added to the summation of weighted inputs, as presented in Eq. (6). Generalized algebraic matrix operations are also given in Eq. (7) to clarify the mathematical operations in an artificial neuron.

$$U_k = Bias_k + \sum_{j=1}^{n} w_{kj} I_j \tag{6}$$

$$U_k = \begin{bmatrix} w_{11} & w_{12} & \cdots & w_{1n} \\ w_{21} & \cdot & & \cdot \\ \cdot & & \cdot & \cdot \\ \cdot & & \cdot & \cdot \\ w_{m1} & \cdots & & w_{mn} \end{bmatrix}_{m\times n} \begin{bmatrix} I_1 \\ I_2 \\ \cdot \\ \cdot \\ I_n \end{bmatrix}_{n\times 1} + \begin{bmatrix} Bias_1 \\ Bias_2 \\ \cdot \\ \cdot \\ Bias_m \end{bmatrix}_{m\times 1} = \begin{bmatrix} U_1 \\ U_2 \\ \cdot \\ \cdot \\ U_m \end{bmatrix}_{m\times 1} \tag{7}$$

In the current study, neural network fitting tool (nftool) provided as a soft-computing tool in MatlabV.R2012a was utilized to perform neural network modelling. In fitting problems, a neural network is used to map between a data set of numeric inputs and a set of numeric targets. The nftool helps create and train a network, and evaluate its performance using mean square error and regression analysis. A two-layer feed-forward network with sigmoid hidden neurons and linear output neurons can fit multi-dimensional mapping problems arbitrarily well, given consistent data and enough neurons in its hidden layer. The network is trained with Levenberg–Marquardt back propagation algorithm [34].

Table 4
Normalization coefficients for the database.

Normalization parameters	Input and output variables				
	D (mm)	t (mm)	L_v (mm)	f_y (MPa)	s_{exp}
β_{max}	600	12.53	3000	1398	1.44
β_{min}	31.76	0.9	300	190	0.68
a	0.00352	0.171969	0.000741	0.001656	2.638396
b	1.111784	1.154772	1.222222	1.31457	2.794109

Since nftool uses the normalized values in the range of $[-1, 1]$, the input parameters were normalized by means of Eq. (8) in order to get the prediction results after execution of the training process of the NN. Additionally, the obtained results are in the normalized form. Therefore, considering Eq. (8) and the normalization coefficients a and b for outputs, de-normalization process is applied and the results are monitored.

$$\beta_{\text{normalized}} = a\beta + b \tag{8}$$

where β is the actual input parameter or output values given in Table 2. $\beta_{\text{normalized}}$ is the normalized value of input parameters or outputs ranging between $[-1,1]$. a and b are the normalization coefficients given in the following equations (Eqs. (9) and (10)).

$$a = \frac{2}{\beta_{\max} - \beta_{\min}} \tag{9}$$

$$b = -\frac{\beta_{\max} + \beta_{\min}}{\beta_{\max} - \beta_{\min}} \tag{10}$$

where $\beta_{\max}$ and $\beta_{\min}$ are the maximum and minimum actual values of either inputs or outputs, respectively. The normalization

Table 5
GEP parameters used for the model derivation.

P1	Function set	+, −, ∗, /, √, \widehat, ln, log, exp, tan, arctan, sin, cos, tanh
P2	Number of generation	469337
P3	Chromosomes	30
P4	Head size	8
P5	Linking function	Addition
P6	Number of genes	10
P7	Mutation rate	0.044
P8	Inversion rate	0.1
P9	One-point recombination rate	0.3
P10	Two-point recombination rate	0.3
P11	Gene recombination rate	0.1
P12	Gene transposition rate	0.1

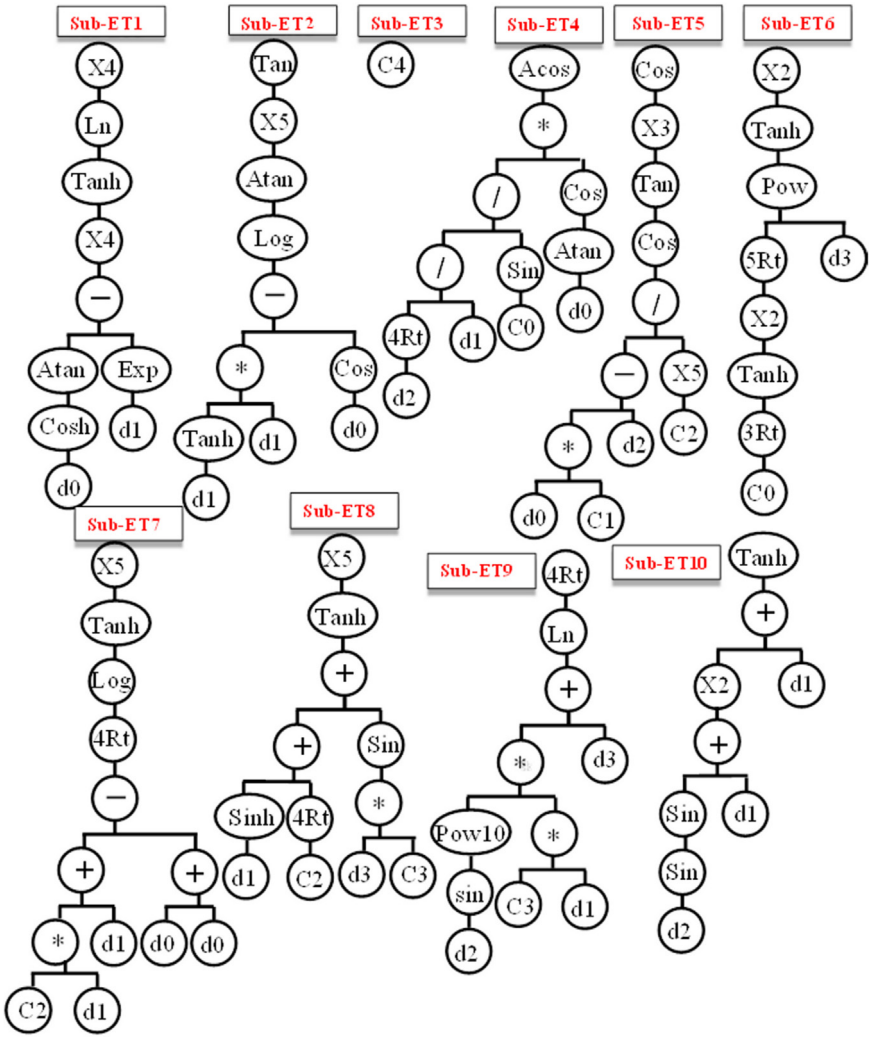

Fig. 5. Expression tree (ET) for the GEP model [d_0: Diameter of CHS, D in mm, d_1: Wall thickness of CHS, t, in mm, d_2: Shear length, L_v, the shear length, being equal to $L/2$ for 3PBT, $(L_1-L_2)/2$ for 4PBT and PBT, and L for CBT where L, L_1, L_2 are described in Fig. 3, in mm, d_3: Yield strength, f_y, in MPa, c_0–c_2: constants].

coefficients for both input and output variables are given in Table 4.

5. Proposed models

5.1. GEP model

The prediction model derived from GEP is presented in Eq. (11). The GEP parameters used for derivation of the mathematical models are given in Table 5. As it can be seen from Table 5, in order to provide an accurate model, various mathematical operations with 10 genes were used. Each gene corresponds to 1 separate expression tree (ET) illustrated in Fig. 5. The ET enables the user to perceive quicker and more complete comprehension of mathematical/logical intricacies. The genes or expression trees are linked to the whole model by addition. Therefore, to find out a prediction value, the input parameters are substituted in the sub-expression functions given in Eqs. (11a)–(11j) and summed as given in Eq. (11), where it should be noted that all trigonometric functions are expressed in radian units.

The most important advantage of this model can be considered as the values are utilized as they are, i.e., there is no need for normalization or any other conversion.

The performance of the proposed GEP model expressed in Eq. (11) is depicted in Fig. 6 for both training and testing data sets. As it can be noted, there is a good trend in the variation of the data between predicted and experimental data especially for the training data. However, the plot indicates similar scatter of the data for the testing database as well. This can be considered as an evidence for the consistency and good fitness of the proposed model.

$$s = s_1 + s_2 + s_3 + s_4 + s_5 + s_6 + s_7 + s_8 + s_9 + s_{10} \tag{11}$$

$$s_1 = \left(\ln\left[\tanh\left(\left[\arctan(\cosh(D) - e^{t})\right]^4\right)\right]\right)^4 \tag{11a}$$

$$s_2 = \tan\left[(\arctan(\log(\tanh(t) \times t - \cos(D))))^5\right] \tag{11b}$$

$$s_3 = -3.431152 \tag{11c}$$

$$s_4 = \arccos\left[\frac{(L_v)^{1/4}}{t \times \sin(10.293854)} \times \cos(\arctan(D))\right] \tag{11d}$$

$$s_5 = \cos\left[\left(\tan\left(\cos\left(\frac{L_v - D \times 15.656647}{27570.05}\right)\right)\right)^3\right] \tag{11e}$$

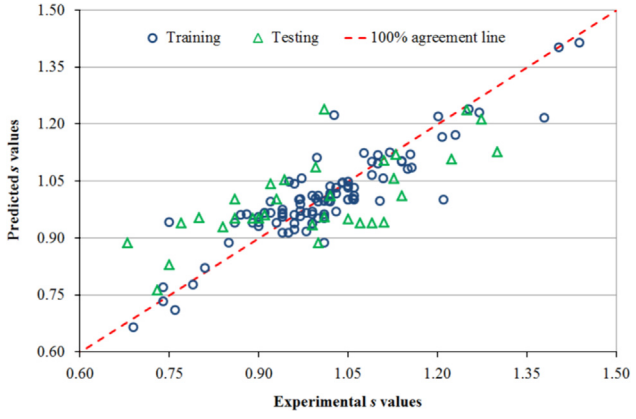

Fig. 6. Experimental vs. predicted flexural overstrength factors using the GEP model.

$$s_6 = \left[\tanh\left((0.9931176)^{f_y}\right)\right]^2 \tag{11f}$$

$$s_7 = \left[\tanh\left(\log\left((t \times 19.986908 + L_v - 2 \times D)^{1/4}\right)\right)\right]^5 \tag{11g}$$

$$s_8 = \left[\tanh\left(\sinh(t) + 1.21165407 + \sin(-9.761414 \times f_y)\right)\right]^5 \tag{11h}$$

$$s_9 = \left[\ln\left(10^{\sin(L_v)} \times t \times 5.509308 + f_y\right)\right]^{1/4} \tag{11i}$$

$$s_{10} = \tanh\left[(\sin(\sin(L_v)) + t)^2 + t\right] \tag{11j}$$

5.2. NN model

A 4-20-1 NN architecture (i.e. 4 inputs – 20 neurons – 1 output) was used to derive the NN model, as shown in Fig. 7. The 4 nodes used in the input layer correspond to D, t, L_v; and f_y, while 20 nodes in the hidden layer, and one in the output layer corresponding to the flexural overstrength factor of CHS beams. The optimum number of nodes in hidden layer was determined based on the preliminary trial-error study which yielded the minimum mean square error and highest correlation coefficient (R) for both training and testing database.

The NN model and corresponding mathematical operations are given in Eqs. (12)–(15). It should be noted that all numeric variables were normalized to a range of $[-1, 1]$ before being introduced to the NN. Therefore, one must enter the normalized values in the mathematical operations given for the NN model. The final result obtained from Eq. (12) is also in the normalized form which needs to be de-normalized according to Eq. (8) and normalization coefficients given in Table 3.

$$s = Bias_{output} + \sum_{i=1}^{20} W_i f(U_i) \tag{12}$$

where $Bias_{output\ layer} = 0.17897$ and $f(x)$ (Hyperbolic tangent) is the activation function given in Eq. (13), U_k given in Eq. (14), and W_k is the layer weight matrix given in Eq. (15)

$$f(x) = \tanh(x) \tag{13}$$

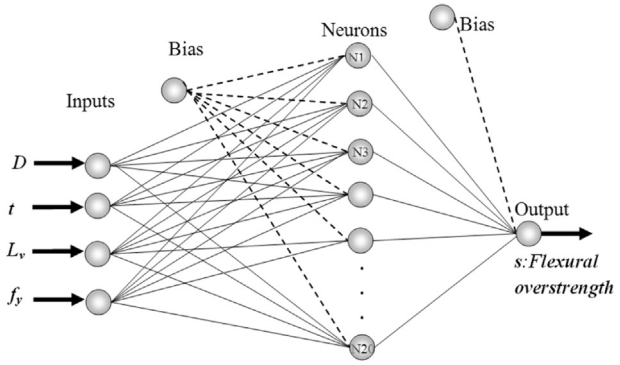

Fig. 7. Architecture of the NN model.

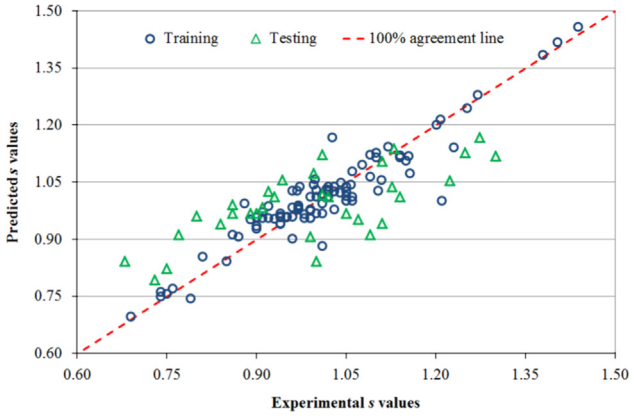

Fig. 8. Experimental vs. predicted flexural overstrength factors using the NN model.

$$U_k = \begin{bmatrix} 1.951 & 1.605 & -1.0977 & 0.17684 \\ 0.32634 & 2.8507 & 0.39365 & 0.97529 \\ 2.2453 & 0.63962 & 0.71347 & -1.6176 \\ 2.0716 & -0.32527 & 1.8286 & 1.2696 \\ 0.77938 & -2.36 & 0.74443 & 1.0994 \\ -1.5204 & 4.0457 & 0.21421 & 0.11422 \\ -2.3956 & -0.14329 & 1.4099 & -1.4246 \\ -2.0839 & -2.2982 & -0.82874 & 2.9624 \\ -2.6078 & 4.6385 & 2.3884 & -5.353 \\ 2.3783 & -1.0717 & 0.24263 & -0.90986 \\ -4.3448 & 0.57855 & 3.1894 & 2.0171 \\ -2.2319 & -1.1951 & -0.09495 & -0.77466 \\ -3.8304 & 0.36479 & 2.0087 & 1.107 \\ -0.9968 & -0.2556 & 2.0761 & 2.1999 \\ 1.4218 & 0.67094 & -2.1798 & -2.3835 \\ 2.0012 & 3.5595 & -0.51361 & -0.51654 \\ 2.172 & 0.43805 & 0.95872 & -2.719 \\ 3.6783 & 2.2704 & 1.0248 & -0.54403 \\ -0.59241 & 0.46593 & 1.78332 & -2.6824 \\ 0.53643 & -0.22997 & -2.0519 & -2.0632 \end{bmatrix} \times \begin{bmatrix} D \\ t \\ L_v \\ f_y \end{bmatrix} + \begin{bmatrix} -3.3375 \\ -2.513 \\ -2.5924 \\ -2.0746 \\ -1.3549 \\ -0.24423 \\ 1.6634 \\ -0.38079 \\ 2.4735 \\ -0.80422 \\ -0.053994 \\ -0.49991 \\ -1.3821 \\ -1.2878 \\ -0.037101 \\ 1.5553 \\ 2.7481 \\ 1.7538 \\ -2.731 \\ 2.9453 \end{bmatrix} = \begin{bmatrix} U_1 \\ U_2 \\ U_3 \\ U_4 \\ U_5 \\ U_6 \\ U_7 \\ U_8 \\ U_9 \\ U_{10} \\ U_{11} \\ U_{12} \\ U_{13} \\ U_{14} \\ U_{15} \\ U_{16} \\ U_{17} \\ U_{18} \\ U_{19} \\ U_{20} \end{bmatrix} \quad (14)$$

$$W_k = \begin{bmatrix} W_1 \\ W_2 \\ W_3 \\ W_4 \\ W_5 \\ W_6 \\ W_7 \\ W_8 \\ W_9 \\ W_{10} \\ W_{11} \\ W_{12} \\ W_{13} \\ W_{14} \\ W_{15} \\ W_{16} \\ W_{17} \\ W_{18} \\ W_{19} \\ W_{20} \end{bmatrix} = \begin{bmatrix} 0.071122 \\ 1.1137 \\ 0.22354 \\ -0.91295 \\ 0.25733 \\ 0.37255 \\ 0.043539 \\ -0.29602 \\ 1.639 \\ -0.060476 \\ -1.4157 \\ 0.59497 \\ 2.1436 \\ -0.73001 \\ -2.5828 \\ -0.03119 \\ 0.99933 \\ -0.43068 \\ -0.42762 \\ 0.39589 \end{bmatrix} \quad (15)$$

The obtained results from the NN model are also plotted in Fig. 8 indicating closer trend than that of the GEP model for both training and testing data sets. Since the estimated values are very close to the 100% agreement line, it can be inferred that the proposed NN model has lower error and higher accuracy than the proposed GEP model.

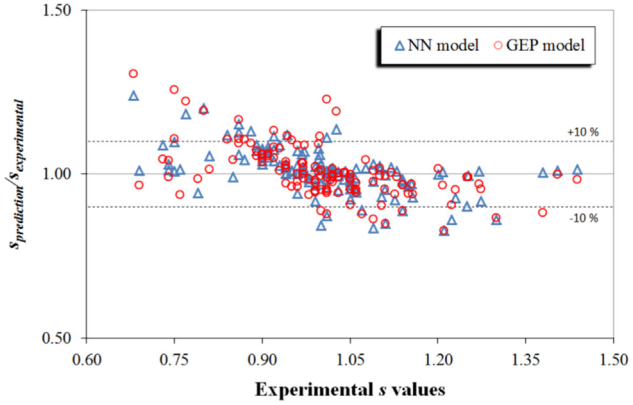

Fig. 9. Comparison of the prediction capability of the NN and GEP models.

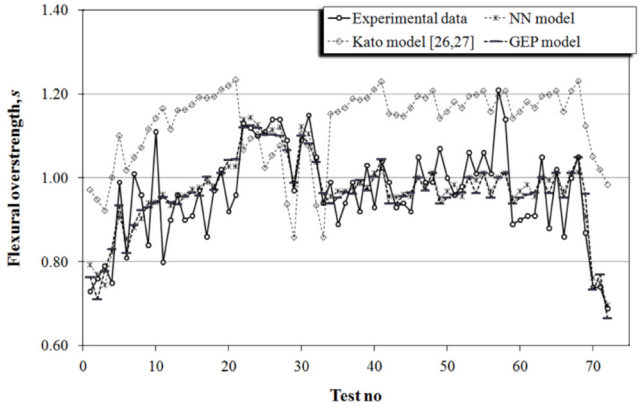

Fig. 10. Prediction performance of the proposed models vs. Kato model for cold-formed CHS beams.

6. Performance of the proposed models

Fig. 9 shows the comparison of the performance of both proposed models in terms of the normalized values ($s_{prediction}$/ $s$experimental) versus the corresponding experimental values ($s_{experimental}$) in order to indicate the accuracy of the prediction. The most accurate prediction performance corresponds to the normalized value equal to 1.0, which is the perfect estimation. Fig. 9 clearly shows that the closest trend in variation of the normalized values around 1 was observed for the NN model especially for the observed s values ranging between 0.9 and 1.05. Although for both of the proposed models the tendency of the normalized values is to slightly underestimate the performance as the $s_{experimental}$ increases, for the most three outer s values in the data set the estimation performance of NN model was almost excellent (normalized values are 1.004, 1.013, 1.010). The lowest and the highest outer normalized values were obtained exactly at the same s value for both of the model. For $s=1.21$ both the GEP and NN models yielded normalized s value of 0.82, while for $s=0.68$ GEP and NN models yielded normalized s values of 1.30 and 1.24, respectively.

The effectiveness of the proposed models has been also verified against the analytical model given by Kato [26,27]. With this aim, Fig. 10 depicts the experimental s values versus the predicted values by the proposed models and the Kato model [26,27] for each corresponding data sample. Since Kato model was developed from the experimental data obtained from the cold-formed steel beams, the model was only applied to the data samples taken from the studies by [14–17,20,21]. Therefore, 72 data samples were used for this comparison. Fig. 10 revealed that Kato model [26,27] generally overestimate the performance (for 62 data samples). Only few data were close to or less than the actual s values.

Fig. 11 shows the average absolute errors for the specific intervals of experimental s values compared in Fig. 10. The average errors calculated for both proposed models were very close to each other regardless the s values, while the errors for Kato model [26,27] decreased as the s values increased. The highest average error for Kato model was about 34.5% at $0.6 < s \leq 0.8$, whereas the errors of the proposed models were about 5% for all intervals.

The interaction of the prediction parameters with the performance of the proposed models are graphically summarized in Fig. 12. Similarly to Fig. 9, the normalized values were utilized for comparison purpose. The plots presented in Fig. 12 showed that although there was accumulation of data for each parameter, the predicted values had various scatters of overestimation and underestimation performance. This case could be considered as evidence that the proposed models are not strictly dependent on a specific parameter. All four parameters were fairly effective and the proposed models had general estimation capability.

Finally, in order to make further evaluation of the performance of the prediction models, the following statistical parameters were computed and reported in Table 6.

$$\text{Mean absolute percent error} \quad \text{MAPE} = \frac{1}{n}\sum_{i=1}^{n}\left|\frac{m_i - p_i}{m_i}\right| \times 100 \qquad (16)$$

$$\text{Mean square error;} \quad \text{MSE} = \frac{\sum_{i=1}^{n}(m_i - p_i)^2}{n} \qquad (17)$$

$$\text{Root mean square error;} \quad \text{RMSE} = \sqrt{\frac{\sum_{i=1}^{n}(m_i - p_i)^2}{n}} \qquad (18)$$

where m and p are values of measured (m_i) and predicted (p_i) values, respectively.

As clearly observed in Table 6, even though error values calculated for both models were close to each other, the correlation coefficients calculated for the NN model were considerably higher than that of the GEP model. Therefore, the strength of the relationship between the predicted values and actual values for the NN model was more than that of the GEP model.

7. Conclusions

Soft computing based modelling approaches for the explicit formulation of flexural overstrength factor of circular hollow section (CHS) beams made of cold-formed, hot formed or fabricated steel is presented in this study. The proposed models are derived using two soft-computing techniques, namely gene expression programming (GEP) and artificial neural networks (NN). To this aim, available experimental data presented in the existing literature were used to develop the models. In order to evaluate their efficiency, the performance of the proposed models was compared to both experimental data and to the analytical model provided by Kato [26,27]. Based on the analysis of the results, the following conclusions can be drawn:

- Both neural network and genetic programming could be handful tools to generate effective mathematical formulations of flexural overstrength factor of circular hollow section steel beams having different geometrical and mechanical properties.
- The level of correlation coefficients and the calculated error values of the proposed models are satisfactory for prediction purposes. The correlation coefficients for training database are 0.89 and 0.94 for the GEP and NN models, respectively. Moreover, for testing databases very close correlation coefficients of 0.70 for the former and 0.71 for the latter are achieved. It is worth noting that although the database for testing data set were not used for training, high level of prediction was obtained for both training and testing data sets associated with low mean absolute percentage of error and high coefficients of correlation. This can be attributed to the generalization capability of the developed model.
- Even though statistical analysis based on MAPE and MSE values reveals that both of the proposed GEP and NN formulations have very close values, thorough observation of the overall tendency of the estimation performance suggests that NN model may be considered as more preferable one.
- The comparison of the proposed models with the model proposed by Kato [26,27] points out that the proposed models provide a better prediction capability.

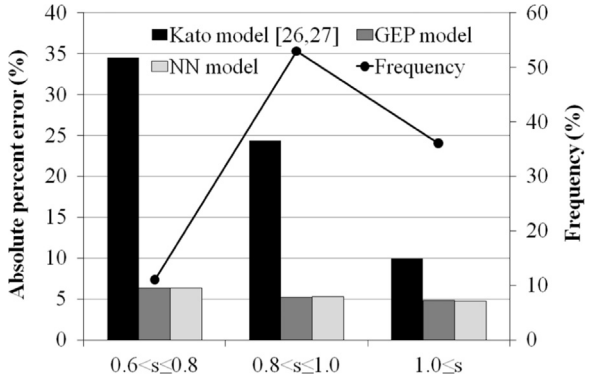

Fig. 11. Mean absolute errors obtained from the NN, GEP, and Kato models for different intervals.

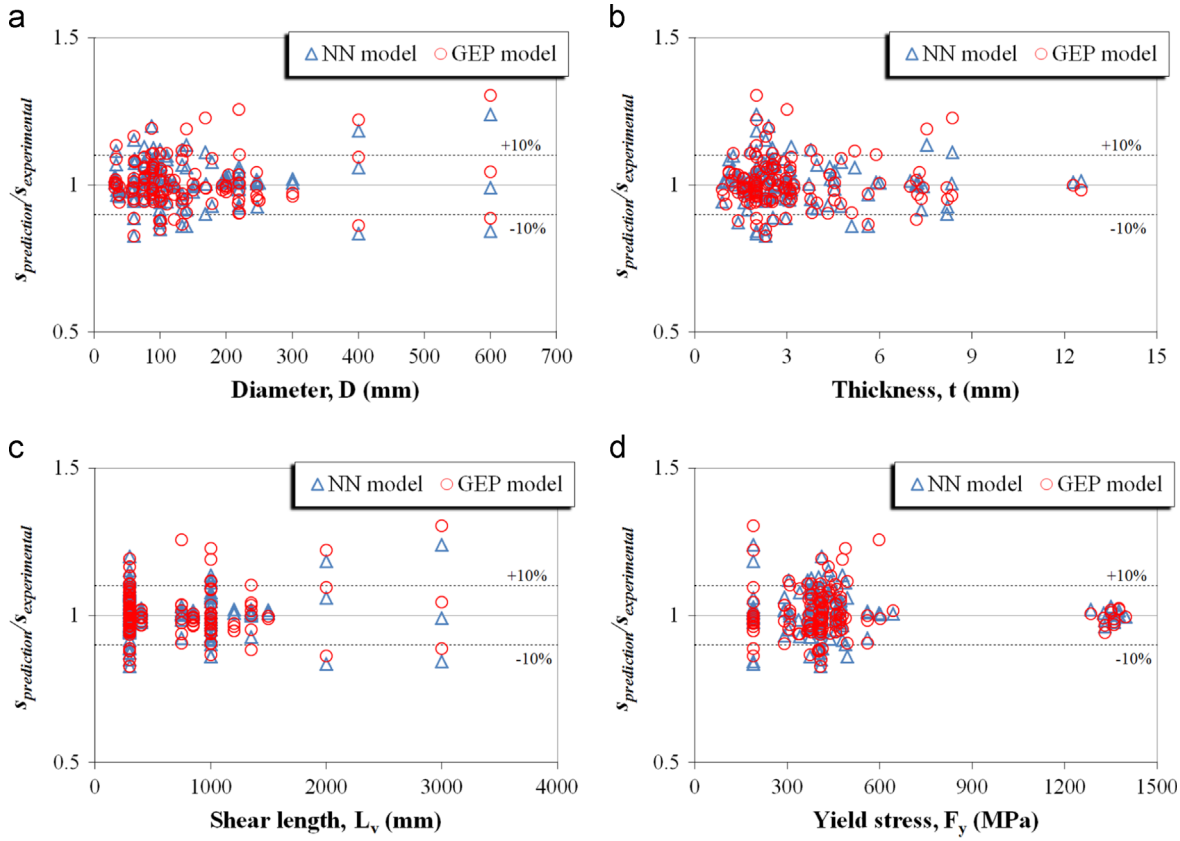

Fig. 12. Interaction of the proposed models with (a) the diameter of the section, (b) the thickness of the section, (c) the shear length, and (d) the yield stress.

Table 6
Statistical parameters of the proposed models.

Model	MAPE		MSE		RMSE		*R*	
	Train	Test	Train	Test	Train	Test	Train	Test
GEP model	4.31	10.28	0.0035	0.0127	0.0593	0.1128	0.89	0.70
NN model	3.27	10.58	0.0021	0.0128	0.0462	0.1134	0.94	0.71

References

[1] Lee Chin-Hyung, Baek Jeong-Hoon, Chang Kyong-Ho. Bending capacity of girth-welded circular steel tubes. J Constr Steel Res 2012;75:142–51.
[2] Chang Kao-Hua, Pan Wen-Fung. Buckling life estimation of circular tubes under cyclic bending. Int J Solids Struct 2009;46:254–70.
[3] Lee Kuo-Long, Pan Wen-Fung, Kuo Ju-Nan. The influence of the diameter-to-thickness ratio on the stability of circular tubes under cyclic bending. Int J Solids Struct 2001;38:2401–13.
[4] Elchalakani M, Zhao XL, Grzebieta RH. Plastic mechanism analysis of circular tubes under pure bending. Int J Mech Sci 2002;44:1117–43.
[5] D'Aniello M, Landolfo R, Piluso V, Rizzano G. Ultimate behavior of steel beams under non-uniform bending. J Constr Steel Res 2012;78:144–58.
[6] Mazzolani FM, Piluso V. Evaluation of the rotation capacity of steel beams and beam-columns. In: Proc. of COST C1 workshop, Strasbourg; October 28–30, 1992.
[7] Mazzolani FM, Piluso V. Theory and design of seismic resistant steel frames. London: E & FN Spon an imprint of Chapman & Hall; 1996.
[8] Wilkinson T, Hancock G. Predicting the rotation capacity of cold-formed RHS beams using finite element analysis. J Constr Steel Res 2002;58:1455–71.
[9] Gioncu V, Mosoarca M, Anastasiadis A. Prediction of available rotation capacity and ductility of wide-flange beams part 1: DUCTROT-M computer program. J Constr Steel Res 2012;69:8–19.
[10] Anastasiadis A, Mosoarca M, Gioncu V. Prediction of available rotation capacity and ductility of wide-flange beams part 2: applications. J Constr Steel Res 2012;68:176–91.
[11] D'Aniello M, Güneyisi EM, Landolfo R, Mermerdaş K. Analytical prediction of available rotation capacity of cold-formed rectangular and square hollow section beams. Thin Walled Struct 2014;77:141–52.
[12] Güneyisi EM, D'Aniello M, Landolfo R, Mermerdaş K. A novel formulation of the flexural overstrength factor for steel beams. J Constr Steel Res 2013;90:60–71.
[13] Güneyisi EM, D'Aniello M, Landolfo R, Mermerdaş K. Prediction of the flexural overstrength factor for steel beams using artificial neural network. Steel Compos Struct 2014;17(3):215–36.
[14] Sedlacek G., Dahl W., Stranghöner N., Kalinowski B, Rondal J., Boeraeve P.H. Investigation of the rotation behaviour of hollow section beams, European Commission, Technical Steel Research, contract no: 7210-SA/119, final report; 1998.
[15] Elchalakani M, Zhao XL, Grzebieta RH. Bending tests to determine slenderness limits for cold-formed circular hollow sections. J Constr Steel Res 2002;58(11):1407–30.
[16] Elchalakani M, Zhao XL, Grzebieta RH. Plastic slenderness limit for cold-formed circular hollow sections. Aust J Struct Eng 2002;3(3):127–39.
[17] Jiao H, Zhao XL. Section slenderness limits of very high strength circular steel tubes in bending. Thin Walled Struct 2004;42:1257–71.
[18] Elchalakani M, Zhao XL, Grzebieta RH. Cyclic bending tests to determine fully ductile slenderness limits for cold-formed circular hollow sections. J Struct Eng, ASCE 2004;127(7):1001–10.
[19] Kiymaz G. Strength and stability criteria for thin-walled stainless steel circular hollow section members under bending. Thin Walled Struct 2005;43:1534–49.
[20] Elchalakani M, Zhao XL, Grzebieta RH. Variable amplitude cyclic bending tests to determine fully ductile slenderness limits for cold-formed circular hollow sections. Eng Struct 2006;28(9):1223–35.
[21] Haedir J, Bambach MR, Zhao XL, Grzebieta RH. Strength of circular hollow sections (CHS) tubular beams externally reinforced by carbon FRP sheets in pure bending. Thin Walled Struct 2009;47:1136–47.
[22] Guo L, Yang S, Jiao H. Behavior of thin-walled circular hollow section tubes subjected to bending. Thin Walled Struct 2013;73:281–9.
[23] Kiymaz G, Coskun E, Cosgun C. Behavior and design of seam-welded stainless steel circular hollow section flexural members. J Struct Eng 2007;133(12):1792–800.
[24] Shahin MA, Elchalakani M. A new model based on evolutionary computing for predicting ultimate pure bending of steel circular tubes. J Constr Steel Res 2014;94:84–90.
[25] Shahin MA, Elchalakani M. Neural network for modelling ultimate pure bending of steel circular tubes. J Constr Steel Res 2008;64:624–33.
[26] Kato B. Rotation capacity of H-section members as determined by local buckling. J Constr Steel Res 1989;13:95–109.

[27] Kato B. Rotation capacity of steel members subject to local buckling. In: Proc. of ninth world conference on earthquake engineering, paper 6-2-3, Tokyo-Kyoto; 1988.
[28] Zadeh LA. Soft-computing and fuzzy logic. IEEE Softw 1994;11(6):48–56.
[29] Koza JR. Genetic programming: on the programming of computers by means of natural selection. MIT Press; 1992.
[30] Goldberg D. Genetic Algorithms in search, optimization and machine learning. MA: Addison-Welsley; 1989.
[31] Ferreira C. Gene expression programming: a new adaptive algorithm for solving problems. Complex Syst 2001;13(2):87–129.
[32] Zhang Z, Friedrich K. Artificial neural networks applied to polymer composites: a review. Compos Sci Technol 2003;63:2029–44.
[33] Wasserman PD. Neural computing theory and practice. New York, USA: Van Nostrand Reinhold Co.; 1989.
[34] Levenberg K. A method for the solution of certain non-linear problems in least squares. Q Appl Math 1944;2:164–8.